34th AIAA Fluid Dynamics Conference and Exhibit, 28 Jun – 1 Jul, Portland, Oregon

Semi-implicit Preconditioning for Wall-bounded Flow.

Christian Wollblad, Lars-Erik Eriksson and Lars Davidson
Division of Thermo and Fluid Dynamics
Chalmers University of Technology
SE-412 96 Göteborg, Sweden

Large eddy simulations (LES) of high speed compressible viscous flow require high space resolution as well as short time steps if explicit time stepping is used. A semi-implicit preconditioning scheme specially suitable for wall-bounded flow is developed which, when combined with an explicit time stepping algorithm, makes much larger time steps possible than with the explicit scheme alone. The method is validated for developing turbulent channel flow and applied to a transonic flow with shock wave turbulent boundary layer interaction. In both cases, the computational time saved is measured. Finally possible developments of the method are discussed.

Nomenclature

ρ	**density**
u, v, w	**velocities in x- , y- and z- directions, also denoted u_1, u_2 and u_3**
e_0	**total internal energy**
h_0	**total enthalpy**
p	**pressure**
q_1, q_2, q_3	**heat transfer in x- , y- and z- directions**
μ	**dynamic viscosity**
δ_{ij}	**the Kronecker delta**
Δt	**time step size**
$\Delta x, \Delta y, \Delta z$	**cell length, height and width**
a	**speed of sound**
u_*	**friction velocity**
δ_{99}	**distance from the wall where mean velocity is 99 % of the free-stream velocity**
ν	**kinematic viscosity**
$\langle u_i u_j \rangle$	**(resolved) Reynolds stress tensor components**
M	**Mach number**
T	**temperature**
T_r	**recovery temperature**
r	**recovery factor**

Subscripts

i, j, k	**cell indices**
∞	**free-stream condition**
0	**total quantity**
w	**wall condition**
p	**profile data**
m	**measured data**

Conventions

Nodes and cells.	**The grids, which are structured grids, are built up from nodes. A cell consists of eight nodes, one in each corner. The flow data is represented as averages over these cells.**

Superscripts

$+$	**wall friction unit**
$\hat{}$	**discretized quantity**

I. Introduction

Shock wave turbulent boundary layer interactions (SWTBLI) have drawn attention for quite a long time.[1] There is an interest to be able to predict the formation of shocks and eventual separation that might occur where the shock interacts with the boundary layer. Such situations commonly arise in the field of turbo machinery, aero-space applications and on the exterior of high-speed aircrafts. In all of these cases, shock wave boundary layer interaction can significantly change the flow and hence the physical load enforced by it. Also, the performance of the object studied can be significantly altered if shocks and boundary layer separations do not occur where expected.

Many experimental studies of SWTBLI have been performed and some basic understanding of the phenomena has been achieved. But much of the results regarding details in the flow can be questioned because of the intrusive nature of the experiments.[1] In recent years, new non-intrusive techniques such as PIV and LDA have been introduced and show great promise. Some numerical studies of SWTBLI have been produced (see for example Ref. 2), but the high computational capacity required to perform something else but Reynolds Averaged Navier Stokes (RANS) calculations, make results from more advanced calculations sparse.

In this work, transonic flow over a bump (see section V) is studied. Such a flow, and most flows including shock wave boundary layer interactions, includes many structures which are hard to capture with RANS methods. This is particularly true for separation and recirculation.[3,4] Because of the problems connected to RANS, Large Eddy Simulation (LES) seems to be a better choice. The problem is then the high computational costs. The flow includes a boundary layer which requires very high near-wall resolution and, for explicit time stepping, small time steps. The strongest constraint on the time step is, for wall bounded compressible flow, always set by the cells closest to the wall.

A general rule for all numerical methods is that they can be made more efficient the more information that are put into them. Using the knowledge about what cells are limiting the time step, a method for taking larger time steps will here be presented. This idea is in no way new. Another version has been implemented by Dong and Zhong[5] for Direct Numerical Simulation (DNS) of compressible supersonic flow. They used the concept of operator splitting which have been used for a long time in for example chemical reacting flows where the stiff terms, normally the chemical reactions, are separated from other terms enabling much larger time steps to be taken (see for example Ref. 6). Here, another approach is used, with resulting equations that are partly the same but implemented in a different way. The current method is verified for developing channel flow and applied to transonic flow over a bump. Last, some possibilities for further development of the method will be discussed.

II. LES numerics

The solver for the Navier-Stokes equations is based on the G3D series of codes developed by Lars-Erik Eriksson.[7] The versions of the continuity, momentum and energy equa-

tions governing viscous compressible flow, solved by the code, can be written in the form:

$$\frac{\partial}{\partial t}Q + \frac{\partial}{\partial x_i}(F_i - F_{vi}) = 0 \tag{1}$$

where

$$Q = \begin{bmatrix} \rho \\ \rho u_1 \\ \rho u_2 \\ \rho u_3 \\ \rho e_0 \end{bmatrix} \quad F_i = \begin{bmatrix} \rho u_i \\ \rho u_1 u_i + p\delta_{1i} \\ \rho u_2 u_i + p\delta_{2i} \\ \rho u_3 u_i + p\delta_{3i} \\ \rho h_0 u_i \end{bmatrix} \quad F_{vi} = \begin{bmatrix} 0 \\ \tau_{1i} \\ \tau_{2i} \\ \tau_{3i} \\ \tau_{ji}u_j - q_i \end{bmatrix}$$

where in turn

$$\tau_{ij} = -\frac{2}{3}\mu\frac{\partial u_m}{\partial x_m}\delta_{ij} + \mu\left(\frac{\partial u_i}{\partial x_j} + \frac{\partial u_j}{\partial x_i}\right) \tag{2}$$

Note that F_i and F_{vi} can be regarded as functions of Q. This will be used in subsection III.B.

The large eddy formulation is obtained using a box filter of grid-cell size. The filtering is performed implicitly by the discretization scheme. The sub-grid terms are modeled using a compressible version of the Smagorinsky model.[8] For a detailed description of filtering and modeling assumptions see Ref. 9.

III. The Method

A. Why the Need of a new Method?

When discretizising a domain, the grid cells are chosen so that they describe the physics of the flow. It is also desirable to use as few cells as possible to save computational time. Close to a solid wall, the gradients are significantly larger in the wall normal direction than in any other direction. Thus, regarding the objectives just mentioned, the node distance in the wall direction will be much smaller than in any other direction, that is, the cells close to the wall will have high aspect ratio. Also, grids for computation of free shear layers have such cells.

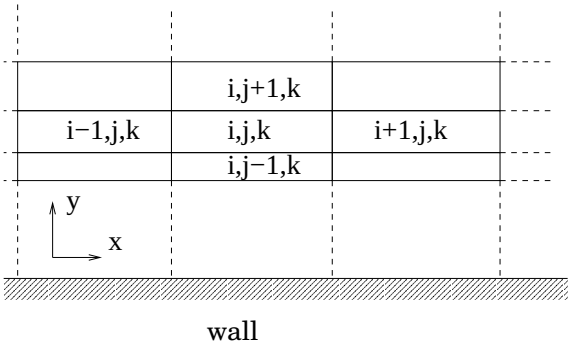

Figure 1. Assumed geometry.

As indicated in figure (1), the focus in this text will be on geometries including solid walls. From here on, we assume that we have a three dimensional domain discretized as shown in figure (1). The discretization in z direction is assumed to be similar to the discretization in the x and y direction. If for example the wall is curved we can always make a coordinate transformation to an orthogonal computational space, see for example Ref. 10. The results will then instead apply to the transformed equations.

The CFL number is a common tool used to choose a time step. For compressible flow, the CFL number of a cell is[11]

$$CFL = |u_{i,j,k}|\frac{\Delta t}{\Delta x} + |v_{i,j,k}|\frac{\Delta t}{\Delta y} + |w_{i,j,k}|\frac{\Delta t}{\Delta z} + a\Delta t\sqrt{\frac{1}{\Delta x^2} + \frac{1}{\Delta y^2} + \frac{1}{\Delta z^2}} \quad (3)$$

which for most explicit numerical schemes should be somewhat less than one for all cells. a is the speed of sound. To resolve an unsteady flow, we need all cells to have the same time step. If we have a flow that is not hypersonic, we can see from equation (3) that for a given Δt, small cells implies large CFL number. Because the very small Δy close to walls, the CFL number will be largest there. Thus, the small Δy close to the wall is limiting the time step for the whole computational domain.

In the case of an instationary flow, there are basically two ways of choosing the time step for a specific explicit time stepping scheme. In this case a second order accurate Runge-Kutta scheme[12] was used even though any similar scheme could have been used. Choosing another scheme, the difference will be the upper limit for the CFL number. The first of the two ways is to use the latest available data and for each cell compute the largest time step allowed. The results are compared and the smallest time step is used for all cells. The second way is to just pick a time step that is small enough. The first way may seem superior in all cases, but due to the implementation of boundary conditions, the second way was used in this work.

Regardless of what way is used to choose the time step, the fact that some cells will have a CFL number much smaller than one remains. As a matter of fact, in many cases, a vast majority of the cells will have a CFL number much smaller than one while only a small fraction of the cells will have CFL number close to the upper limit. Even if a higher order time stepping scheme is used, which allows larger Δt, this situation will remain.

The time has now come to ask the question: What fast flow structures are there close to the wall that we need to resolve and thus are limiting the size of our time step? Once again looking at equation (3), we see that the last term on the right hand side can be large close to the wall despite the no-slip boundary condition. This term represents the small, nearly isotropic sound waves that carry the pressure information. Unless we want to study the sound field, these waves are of no interest. Still we need to know what the effect of their presence is.

This is exactly what can be achieved using implicit time stepping, but using it for the whole domain would not be any more efficient than explicit time stepping. A more efficient approach would be to use some kind of hybrid method where an implicit time stepping is used for cells close to the wall and explicit time stepping scheme is used for other cells. But we can do even better.

B. The Preconditioning Equation

For the present method, the only restriction put on the grid is that it needs to be structured where the method is applied. The flow, on the other hand, must have a region with character such that, for a column of cells, one direction contributes much more to the CFL-number than any other direction. Some other characteristics are also necessary for the method to be of any practical use. These will be described later since they are of no importance for the theoretical derivation of the method.

First the notations

$$\begin{aligned} F_1 &= E, \quad F_{v1} = E_v \\ F_2 &= F, \quad F_{v2} = F_v \\ F_3 &= G, \quad F_{v3} = G_v \end{aligned} \quad (4)$$

are introduced. Applying a finite volume approach using the orthogonality of the grid,

equation (1) for cell i, j, k becomes

$$\begin{array}{lll} & \Delta x\Delta y\Delta z\frac{d}{dt}Q_{i,j,k} + & \\ \Delta y\Delta z & \left(E_{i+1/2,j,k} - E_{i-1/2,j,k} - E_{v\ i+1/2,j,k} + E_{v\ i-1/2,j,k} \right) & + \\ \Delta x\Delta z & \left(F_{i,j+1/2,k} - F_{i,j-1/2,k} - F_{v\ i,j+1/2,k} + F_{v\ i,j-1/2,k} \right) & + \\ \Delta x\Delta y & \left(G_{i,j,k+1/2} - G_{i,j,k-1/2} - G_{v\ i,j,k+1/2} + G_{v\ i,j,k-1/2} \right) & = 0 \end{array} \tag{5}$$

where half valued index indicates an average cell face value. Also note that $Q_{i,j,k}$ is the average value of Q in cell i, j, k. To be fully correct Δx, Δy and Δz should all have index i, j, k, but those have been, and will be for the rest of the chapter, omitted to make the equations more readable. This should cause no confusion.

The continuation from here on depends on the exact discretization scheme used. Even though any discretization scheme can be used, we will in this derivation, for simplicity, use a second order central scheme for both the viscous and the inviscid flux vectors. For example, $E_{i+1/2,j,k}$ will be approximated with $0.5\left(E_{i,j,k} + E_{i+1,j,k}\right)$. Since in this derivation, both the viscous and inviscid fluxes are discretized using the same scheme (which is not necessary in the general case), the fluxes will be written as total fluxes, e.g. $\hat{E}_{t\ i,j,k} = \hat{E}_{i,j,k} - \hat{E}_{v\ i,j,k}$. Using this simplified approach and discretizising the derivatives in the viscous flux vectors, we get from equation (5):

$$\begin{array}{lll} & \Delta x\Delta y\Delta z\frac{d}{dt}\hat{Q}_{i,j,k} + & \\ \frac{1}{2}\Delta y\Delta z & \left(\hat{E}_{t\ i+1,j,k} - \hat{E}_{t\ i-1,j,k} \right) & + \\ \frac{1}{2}\Delta x\Delta z & \left(\hat{F}_{t\ i,j+1,k} - \hat{F}_{t\ i,j-1,k} \right) & + \\ \frac{1}{2}\Delta x\Delta y & \left(\hat{G}_{t\ i,j,k+1} - \hat{G}_{t\ i,j,k-1} \right) & = 0 \end{array} \tag{6}$$

For equation (6), the solution is $\hat{Q}_{i,j,k}$ instead of $Q_{i,j,k}$ which is a solution to the finite volume formulation of the exact equation. The symbol $\hat{}$ on the other terms denotes both that they are functions of $\hat{Q}$ and that all the included terms also are discretized in space.

From here on, the choice normally stands between explicit and implicit time stepping. Let n denote the latest time step for which a solution is available. If explicit time stepping is chosen equation (6) will get the form

$$\begin{array}{lll} & \left(\frac{d\hat{Q}_{i,j,k}}{dt}\right)^{expl.} = & \\ -\frac{1}{2\Delta x} & \left(\hat{E}_t{}^{n}_{i+1,j,k} - \hat{E}_t{}^{n}_{i-1,j,k} \right) & \\ -\frac{1}{2\Delta y} & \left(\hat{F}_t{}^{n}_{i,j+1,k} - \hat{F}_t{}^{n}_{i,j-1,k} \right) & \\ -\frac{1}{2\Delta z} & \left(\hat{G}_t{}^{n}_{i,j,k+1} - \hat{G}_t{}^{n}_{i,j,k-1} \right) & \end{array} \tag{7}$$

where for example $\hat{E}_t{}^{n}_{i+1,j,k} = \hat{E}_t(\hat{Q}^n_{i+1,j,k})$. We have here also introduced the notation

$$\left(\frac{d\hat{Q}_{i,j,k}}{dt}\right)^{expl.} = \frac{\hat{Q}^{n+1,expl.}_{i,j,k} - \hat{Q}^n_{i,j,k}}{\Delta t}.$$

Now we turn our attention to the implicit formulation. We introduce the notation $\hat{Q}^{n+1}_{i,j,k} = \hat{Q}^n_{i,j,k} + \Delta\hat{Q}_{i,j,k}$ which can be used to write the implicit time stepping formulation of equation

(6) as:

$$\begin{array}{rcl} & \left(\frac{d\hat{Q}_{i,j,k}}{dt}\right)^{impl.} + & \\ \frac{1}{2\Delta x} & \left(\hat{E}_t(\hat{Q}^n_{i+1,j,k} + \Delta\hat{Q}_{i+1,j,k}) - \hat{E}_t(\hat{Q}^n_{i-1,j,k} + \Delta\hat{Q}_{i-1,j,k})\right) & + \\ \frac{1}{2\Delta y} & \left(\hat{F}_t(\hat{Q}^n_{i,j+1,k} + \Delta\hat{Q}_{i,j+1,k}) - \hat{F}_t(\hat{Q}^n_{i,j-1,k} + \Delta\hat{Q}_{i,j-1,k})\right) & + \\ \frac{1}{2\Delta z} & \left(\hat{G}_t(\hat{Q}^n_{i,j,k+1} + \Delta\hat{Q}_{i,j,k+1}) - \hat{G}_t(\hat{Q}^n_{i,j,k-1} + \Delta\hat{Q}_{i,j,k-1})\right) & = 0 \end{array} \tag{8}$$

In analogy to above

$$\left(\frac{d\hat{Q}_{i,j,k}}{dt}\right)^{impl.} = \frac{\hat{Q}^{n+1,impl.}_{i,j,k} - \hat{Q}^n_{i,j,k}}{\Delta t}.$$

If now one direction contributes much more to the CFL-number than any other direction, the spectral radius of the overall net flux operator ($\mathcal{H}$ in equation(11)) in that direction, dominates over those of the other directions. Another way to express this is that the coupling between cells in that direction is much stronger than in the other directions. If we for example assume that this is valid for the y-direction, we can make use of this when Taylor expanding equation (8) to neglect all higher order terms that do not represent coupling in the y-direction. If also discarding all terms of second order and higher, we get from equation (8):

$$\begin{array}{rcl} & \left(\frac{d\hat{Q}_{i,j,k}}{dt}\right)^{impl.} + & \\ \frac{1}{2\Delta y} & \left(\left(\frac{\partial\hat{F}_t}{\partial\hat{Q}}\right)^n_{i,j+1,k}\Delta\hat{Q}_{i,j+1,k} - \left(\frac{\partial\hat{F}_t}{\partial\hat{Q}}\right)^n_{i,j-1,k}\Delta\hat{Q}_{i,j-1,k}\right) & = \\ & -\frac{1}{2\Delta x}\left(\hat{E}_t{}^n_{i+1,j,k} - \hat{E}_t{}^n_{i-1,j,k}\right) & \\ & -\frac{1}{2\Delta y}\left(\hat{F}_t{}^n_{i,j+1,k} - \hat{F}_t{}^n_{i,j-1,k}\right) & \\ & -\frac{1}{2\Delta z}\left(\hat{G}_t{}^n_{i,j,k+1} - \hat{G}_t{}^n_{i,j,k-1}\right) & \end{array} \tag{9}$$

Now recall the identity $\Delta\hat{Q}_{i,j,k}/\Delta t = (d\hat{Q}_{i,j,k}/dt)^{impl.}$. When comparing the right hand side of equation (9) with equation (7) we see that equation (9) can be written as:

$$\begin{array}{l} \left(\frac{d\hat{Q}_{i,j,k}}{dt}\right)^{impl.} + \frac{\Delta t}{2\Delta y}\left(\frac{\partial\hat{F}_t}{d\hat{Q}}\right)^n_{i,j+1,k}\left(\frac{d\hat{Q}_{i,j+1,k}}{dt}\right)^{impl.} - \\ \frac{\Delta t}{2\Delta y}\left(\frac{\partial\hat{F}_t}{\partial\hat{Q}}\right)^n_{i,j-1,k}\left(\frac{d\hat{Q}_{i,j-1,k}}{dt}\right)^{impl.} = \left(\frac{d\hat{Q}_{i,j,k}}{dt}\right)^{expl.} \end{array} \tag{10}$$

Equation (10) is a relation between the explicit and implicit time derivative of $\hat{Q}_{i,j,k}$ (see subsection III.C). Observe that the exact form of equation (10) depends on what discretization schemes that are used. But a very important fact remains for all discretization schemes: The coupling between the implicit time derivatives is in the y direction only.

In fact, it can be shown that using equation (10) is equivalent to making one iteration using Newton-Raphson's method for the y-direction. This can be seen if we regard a compact form of equation (6):

$$\frac{dQ}{dt} = \mathcal{H}(Q) \tag{11}$$

where $\mathcal{H}$ then is an operator including all discretized spatial derivatives. The 'hat'-notation and the indices are dropped for readability. An implicit time step formulation of first order in time would be:

$$\frac{Q^{n+1} - Q^n}{\Delta t} = \mathcal{H}(Q^{n+1}) \tag{12}$$

As above, introducing $\Delta Q = Q^{n+1} - Q^n$ and rearranging equation (12) we get:

$$\Delta Q = \Delta t \mathcal{H}(Q^n + \Delta Q) \tag{13}$$

If Q^n is known and Δt is fixed this is an equation for finding ΔQ. Let $\Delta Q = \Delta Q^{(p)} + \delta(\Delta Q)$. We can then transfer the problem of finding a solution to equation (13) to finding a series $\{\delta(\Delta Q)\}_0^\infty$ such that $\Delta Q^{(p+1)} = \Delta Q^{(p)} + \delta(\Delta Q)$ and $\lim_{p\to\infty} \delta(\Delta Q) = 0$. This is Newton-Raphson's method. Inserting into equation (13) and linearizing with respect to $\delta(\Delta Q)$ gives:

$$\begin{gathered} \Delta Q^{(p)} + \delta(\Delta Q) = \\ \Delta t \mathcal{H}(Q^n + \Delta Q^{(p)} + \delta(\Delta Q)) \approx \\ \Delta t \mathcal{H}(Q^n + \Delta Q^{(p)}) + \Delta t \mathcal{H}'(Q^n + \Delta Q^{(p)}) \delta(\Delta Q) \end{gathered} \tag{14}$$

where prime denotes derivation with respect to Q. Now, since $\Delta Q^{(0)}$ is arbitrary we may choose to set it to zero. Inserting into equation (14) and rearranging gives:

$$(I - \Delta t \mathcal{H}'(Q^n)) \delta(\Delta Q) = \Delta t \mathcal{H}(Q^n) \tag{15}$$

where I is the identity matrix. Since $\Delta Q^{(0)} = 0$ we can replace $\delta(\Delta Q)$ with $\Delta Q^{(1)}$. Once again recalling the identity $\frac{\Delta Q}{\Delta t} = \left(\frac{dQ}{dt}\right)$ we may rearrange equation (15) to get:

$$(I - \Delta t \mathcal{H}'(Q^n)) \left(\frac{dQ}{dt}\right)^{(impl.)} = \mathcal{H}(Q^n) = \left(\frac{dQ}{dt}\right)^{(expl.)} \tag{16}$$

To get from here to equation (10), we just have to expand equation (16) and neglect all terms coupling the equations in the x and z direction.

Another interesting observation is that, if we create the equivalence of equation (10) for the x and z direction and apply them in a sequential manner with equation (10), we will get the well known approximate factorization method which in turn is an approximation to a fully implicit scheme.

Both the analogy to Newton-Raphson's method and to the approximate factorization method can be taken as starting points for further development of the current method which will be discussed in the section VI.

C. Time Stepping Scheme

The attentive reader have probably noticed that we so far have used $(\hat{Q}^{n+1} - \hat{Q}^n)/\Delta t$ to approximate $(d\hat{Q}_{i,j,k}/dt)$. But any time stepping scheme can be used. In the derivation, instead of assigning $(d\hat{Q}_{i,j,k}/dt)$ to be anything specific, just think of it as the term from which to calculate $\hat{Q}^{n+1}$ by using some time stepping scheme. Then the relation $\Delta\hat{Q}_{i,j,k}/\Delta t = (d\hat{Q}_{i,j,k}/dt)^{impl.}$, which is used to rewrite equation (9) as equation (10), is an approximation that can easily be derived by expanding $\hat{Q}^{n+1}$ using Taylor's formula.

In this work, we have chosen to use equation (10) for each stage in a three stage, second order accurate Runge-Kutta method. Then $(d\hat{Q}_{i,j,k}/dt)$ is interpreted as the fluxes calculated from the solution obtained in the previous stage. Independent of which time stepping scheme we choose, the preconditioning equation will reduce the spectral radius of the operator $\mathcal{H}$ in equation (11).

D. Implementation

The present method is of interest for wall bounded flow, because of the high aspect ratio of the cells there, equation (10) is valid. Also, for the present method to be of any practical use, the coupling of cells must end somewhere. The more cells that are coupled, the less effective the method will be. In case of a wall, the aspect ratio some distance out from the wall will be much lower than at the wall, and thus there will be no need for semi-implicit preconditioning there.

Utilizing the current method, some terms in equation (3) will change. The terms that represent the contribution from the preconditioned direction, will be replaced by some altered terms. These terms will depend on how equation (10) is implemented. The time step used must be chosen so that this altered CFL-number never gets larger than a limit given by the explicit time step scheme, in our case approximately 0.8.

Equation (10) is implemented by first calculating all uncorrected fluxes for all cells. Since equation (10) couples only cells in the wall normal direction, each 'column' of cells out from the wall can be treated separately in the following way.

1. **Choose a cell close to the wall (not necessarily the one closest to the wall, which have index i, j_{wall}, k) with index i, j, k (see figure (1)).**
2. **Use equation (3) to compute the unaltered CFL number.**
3. **If the result is larger than the largest CFL number allowed, repeat step 2 for the cell with index $i, j + 1, k$.**
4. **We have now found a cell with index $i, j_{max} + 1, k$ for which the CFL number is less than the upper limit for the current explicit time stepping method. Equation (10) applied to each of the cells in a column reaching from i, j_{wall}, k to i, j_{max}, k constitutes a linear equation system with $\left(\frac{d\hat{Q}_{i,j_{wall},k}}{dt}\right)^{impl.}, \ldots, \left(\frac{d\hat{Q}_{i,j_{max},k}}{dt}\right)^{impl.}$ as unknowns. At the adiabatic wall, no-slip boundary condition is used. To calculate the fluxes for the outermost cells in the column, the most recent information from the cells outside the column is used.**
5. **Solve the equation system obtained in step 4 using some method for linear systems. In this work a direct method for band diagonal systems was used. It can be found in Ref. 13.**

Step 1 - 5 is repeated for all wall cells. Then the first stage in the three stage Runge-Kutta method is performed. Before the next stage, all fluxes are recalculated and step 1 through 5 above must be redone for each column. To obtain maximum accuracy, we have chosen also to recalculate all Jacobian matrices in equation (10) for each stage in the Runge-Kutta method.

E. Space Discretization

As mentioned in subsection III.B, equation (10) takes different forms depending on what type of discretization scheme that is used. In this work one scheme is used for the inviscid flux terms and another for the viscous. For the inviscid fluxes a fourth order central scheme with user defined upwinding was used. The upwinding makes the order of the error terms to drop to third order. For the viscous fluxes a second order central scheme was used. See Ref. 14 for more details.

In the case of a shock, the numerical scheme cannot resolve the shock and the resulting instabilities cause divergence of the computation. To hinder this scenario, extra chock capturing diffusion was added. In the calculation of the fluxes, a term based on pressure difference and spectral radius of $\mathcal{H}$ in equation (11) was added. This is described in more detail in Ref. 9.

As can be seen for example in equation (9), we also need discretized Jacobian flux matrices. Both the inviscid and viscous flux Jacobians are calculated by differentiation of the respective flux. For the viscous part, a thin layer approximation[10] is used for the friction work term in the energy equation. Otherwise, the differentiation is exact.

IV. Validation

A. Validation Case Setup

For validation of the accuracy of the method, a simple case, flow between two flat plates was used. The test section was $0.1116\ m$ long, $0.01952\ m$ wide and had a half height of $0.035\ m$.

At the bottom where $y = 0.0\ m$, an adiabatic no-slip boundary condition was imposed and at the top, $y = 0.035\ m$, a symmetry boundary condition was used. For the spanwise direction translational periodic conditions were set. At the inlet a turbulent boundary layer was prescribed. It is described in detail in the subsection V.B. At the outlet, $x = 0.1116$, the static pressure was set $1.0\ kPa$ higher than at the inlet, thus mildly forcing a faster development of the boundary layer.

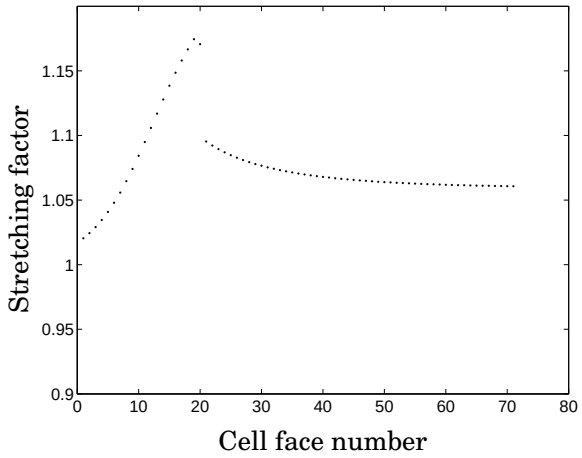

Figure 2. Grid stretching for the validation case.

A further aspect of implementation of the current method is stretching of cells close to the wall. If the cells are not stretched enough, the columns described in subsection III.D will become very long before the CFL-number becomes less than any acceptable limit. On the other hand, the grid cannot be stretched too much without loss of accuracy. In figure (2) the stretching for this particular grid is shown. The maximum stretching at 17.5% is chosen, which is relevant for LES applied to realistic aeronautic applications. For example the DNS used to create the fluctuations for the inlet boundary layer had streaching of such a magnitude. The streching could though be made in a better way and was changed in the test case described in section V.

Two calculations were carried out for this channel. One using fully explicit time stepping and one using the semi-implicit preconditioning scheme. Startup was made from an approximate solution obtained from early test calculations and computations were run for several flow through times (FTTs) to obtain a fully developed flow in time. When the profile of the friction velocity, u_*, had reached a steady mean profile along the channel, which was after about 15 FTTs, the flow field was regarded as fully developed. 511 samples were then taken with large separation in time. Statistics was calculated from those samples and averaged in spanwise direction.

B. Results

The maximum value of y^+ was found at the inlet and was for the first cell face equal to 0.54. At the same location $\Delta x^+ = 81$ and $\Delta z^+ = 14$ and the distance up to $y^+ = 20$ was covered by 17 cells. Thus, the grid can be regarded to have sufficient resolution of the boundary

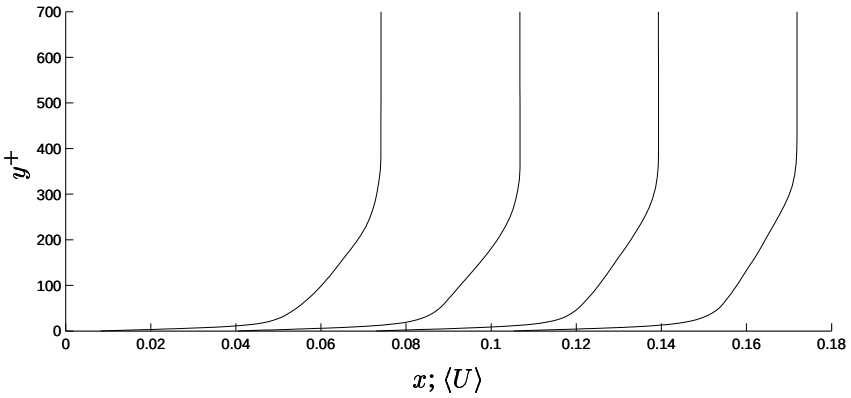

Figure 3. Comparison between the streamwise velocities: —, fully explicit scheme; − −, semi-implicit scheme.

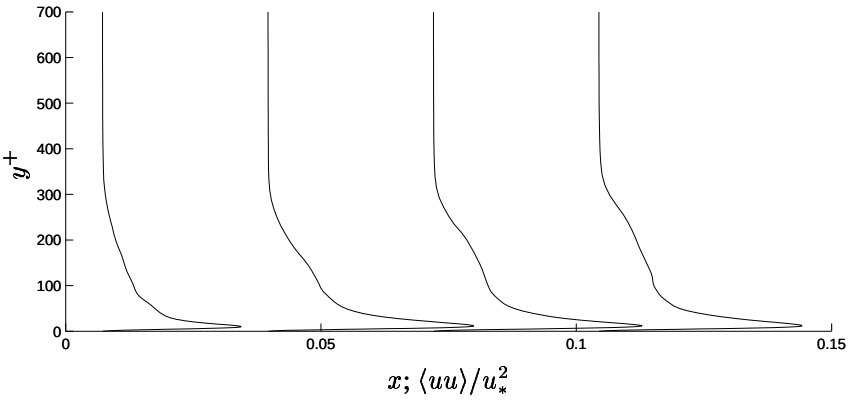

Figure 4. Comparison between the $\langle uu \rangle$ Reynolds stresses: —, fully explicit scheme; − −, semi-implicit scheme.

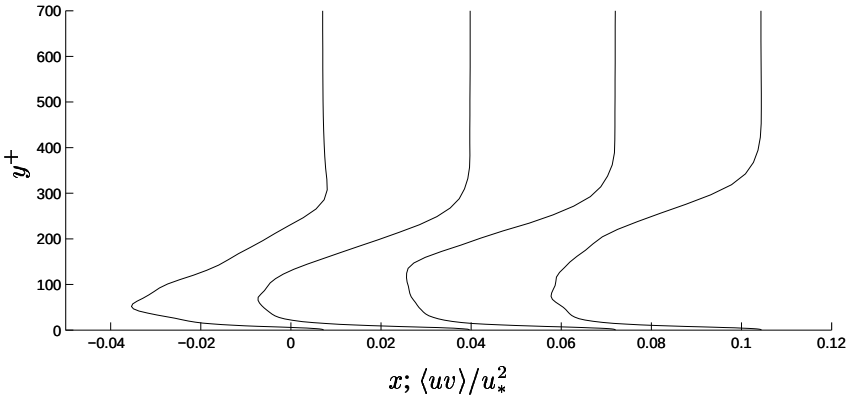

Figure 5. Comparison between the $\langle uv \rangle$ Reynolds stress: —, fully explicit scheme; − −, semi-implicit scheme.

layer structures. No investigations of whether the channel was wide enough was made, but since the objective was to verify that the fully explicit time stepping and the semi-implicit scheme gave the same answer, this was not regarded as necessary.

Figures (3), (4) and (5) show a comparison between the two calculations. None of the figures indicate any deviations at all. The same is true for all Reynold stresses although only two are shown here. Notice that figures (4) and (5) have different scales. The maxi-

mum peak value shown for $\langle uu \rangle / u_*^2$ is 27.2 while the most negative value shown for $\langle uv \rangle / u_*^2$ is -1.88. Tests where only 341 of the 511 samples were used for calculating statistics were performed, but showed merely no deviations at all from statistics calculated from all 511 data sets.

The computational time saved by using the semi-implicit scheme was significant. Despite the fact that a large part of the net was close to a wall and that the grid stretching there was probably not optimal, the semi-implicit scheme used only 60% of the time required by the fully explicit scheme.

With such results, we are comfortable in proceeding to a more difficult test case.

V. A Test Case

A. Test Case Setup

This test case is actually a numerical model of a part of an experimental test rig that is located at the department of energy technology, KTH. The experimental test section is $0.44\ m$ long, $0.10\ m$ wide and $0.12\ m$ high. At the bottom of the test section there is a bump. See Ref. 15 for more details about the rig. Our domain is this test section, but it has been shorten $0.08\ m$ at the outlet and is only $0.019\ m$ wide. Furthermore, the roof has been taken away and is replaced by a symmetry plane. A two-dimensional picture of the domain is shown in figure (6). To mimic the conditions in the test rig as far as possible, the symmetry line is lowered by one momentum loss thickness based on the inlet boundary condition, so that $h = 0.1186154\ m$. In this way, difference in mass displacement between measurements and calculations is prevented to a certain extent. The maximum height of the bump is $0.010477\ m$.

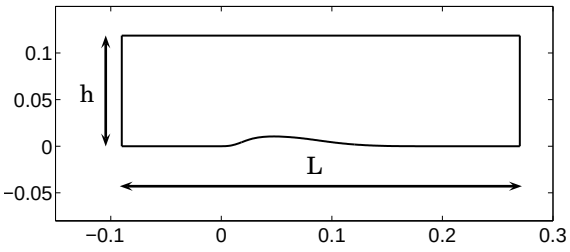

Figure 6. Test case geometry

The geometry is such that for some subsonic boundary conditions at the inlet and outlet, the flow will be accelerated over the bump and the sonic pocket that is formed will be terminated by a shock. Measurements have shown that no shock in the range of interest is so strong that it will reach up to the roof. Therefore, we do not think that replacing the roof with a symmetry plane should have any strong influence on the flow field. A possibility is though that the mass displacement over the bump will be further out in the free-stream if a symmetry line is used compared to a roof, but the reduction of h mentioned earlier should compensate for this.

As mentioned in section IV, the grid stretching could be made better than in the validation case. There, the stretching started at a low rate and increased rapidly and then dropped even quicker. Numerically it would be better to have the grid stretched over a longer distance, avoiding the rather large peak value in the stretching factor. As can be seen in figure (7), this has been done for the test case where the cell stretching in the wall normal direction is shown. Notice that not all cell faces are shown.

An LES simulation with all conditions set as in the experimental rig would be more or less impossible. The Reynolds number based on $h/2$ and the free-stream inlet conditions

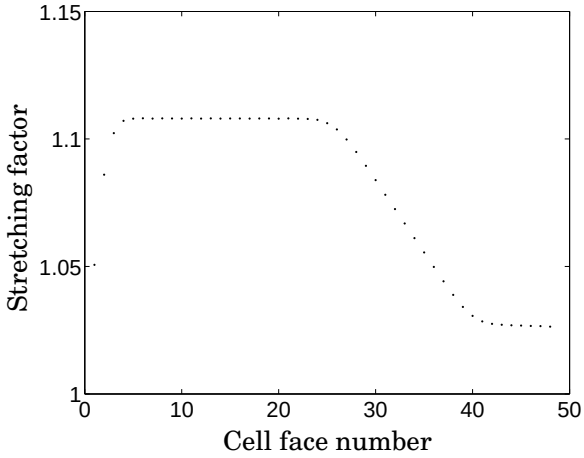

Figure 7. Stretching factor in the wall normal direction for the test case at $x = -0.082\ m$.

would then be about 10^6. The number of nodes needed for such a case is far beyond our capacity today. Therefore we have chosen to decrease the Reynolds number by increasing the viscosity by a factor 11.25 up to $\mu = 1.8e^{-4} Pa\,s$. The boundary layer upstream of the shock is, of course, dependent on the Reynolds number. An effort to compensate for this is made by careful choice of inlet boundary conditions (see next subsection). However, it is better to carry out a well-resolved, accurate LES at a reduced Reynolds number, than an inaccurate LES at the original, high Reynolds number.

B. Boundary Conditions

As already mentioned the upper boundary was set to be a symmetry boundary and as in the validation case, the spanwise boundaries were given translational periodic boundary conditions. Along the wall, no-slip, adiabatic conditions were enforced.

From measurements[16] we know that for free stream inlet boundary conditions of $M = 0.70$, $P_0 = 160.0\ k\,Pa$, $T_0 = 303\ K$ and for some outlet pressure in the range $106 - 107\ k\,Pa$ there will be a shock at the back of the bump. In addition, the inlet should have a turbulent boundary layer. A boundary layer thickness of $8.95\ mm$ was given by a measurement made by Sigfrids,[15] at the location $x = -0.10\ m$ whereas our inlet is at $x = -0.09\ m$ (see figure (6)). Furthermore the measurement was made at a higher Reynolds number due to different viscosity.

An important aspect in the calculations is to match the experimentally obtained boundary layer thickness at the top of the bump, since it determines the acceleration of the flow. There are no simple tools for approximating the development of the boundary layer as it is accelerated over the bump. Instead, a theory for incompressible turbulent boundary layer,[17] was used to calculate the expected boundary layer thickness at the start of the bump, $x = 0.0\ m$, in the test rig. Then, the required δ_{99} at $x = -0.09\ m$ to get the same boundary layer thickness at $x = 0.0\ m$, but with the higher viscosity, was calculated. The calculations gave $\delta_{99} = 8.2\ mm$. Such a profile would have a Reynolds number $Re_\tau = 615$ based on u_* and δ_{99}. Since the development of the boundary layer as it is accelerated up the bump is not included, the boundary layer should be somewhat thinner than the calculated δ_{99}.

A profile for incompressible flow measured by Johansson and Castillo[18] was used but needed rescaling. For a profile with a free stream velocity U_∞ the following relation is

valid:

$$\frac{U}{U_\infty} = f\left(\frac{xU_\infty}{\nu}, \frac{yU_\infty}{\nu}, *\right) \tag{17}$$

where f is some function describing the relation and $*$ denotes the dependence on upstream conditions. Rescaling Johansson's and Castillo's profile using this relation gave a profile with $\delta_{99} = 7.5\ mm$ and $Re_\tau = 632$. Both quantities are close to the desired values.

To get profiles for ρ and ρe_0, the temperature was assumed to followed the Walz' distribution:[19]

$$\frac{T}{T_\infty} = \frac{T_w}{T_\infty} + \frac{T_r - T_w}{T_\infty}\left(\frac{U}{U_\infty}\right) - r\frac{\gamma - 1}{2}M_\infty^2\left(\frac{U}{U_\infty}\right)^2 \tag{18}$$

where T_w is the wall temperature, T_r the recovery temperature and r the recovery factor. From Schlichting we also got that:

$$T_r = T_\infty + r\frac{U_\infty^2}{2c_p} = T_\infty\left(1 + r\frac{\gamma - 1}{2}M_\infty^2\right) \tag{19}$$

and that $r = 0.89$. As the wall was set to be adiabatic, $T_w = T_r$. The pressure was assumed constant through the boundary layer and its value was given by the measurements made by Sigfrids. Combined with the ideal gas law, the desired profiles were obtained.

The fluctuations were taken from incompressible DNS of fully developed channel flow. The data had to be rescaled based on u_*, ν and h_{DNS} versus δ_{99} where h_{DNS} was half the channel height for the DNS calculation. Observe that both space and time variables needed scaling. The pressure fluctuations were based on the dynamic pressure fluctuations from the DNS. Since the DNS was incompressible, the acoustic fluctuations were missing. They are however relatively small and were therefore neglected. Because fully developed channel flow has a much higher turbulent intensity in the middle of the channel than developing boundary layer has in the outer region, the fluctuations from the DNS had to be reduced. A filter was created by comparing RMS data from the DNS and the measurements made by Johansson and Castillo. The filter was applied to the fluctuations before they were added to the inlet profile.

The mathematical form of the inlet boundary condition was that of a nonreflective boundary condition based on flow characteristics where $\rho, \rho u, \rho v, \rho w$ and ρe_0 are given as boundary values. The free stream value of these five were set to $1.3766\ kg/m^3$, $312\ Ns/m^3$, $0.0\ Ns/m^3$, $0.0\ Ns/m^3$ and $310\ kJ/m^3$.

At the outlet, subsonic boundary conditions with static pressure set to $107\ kPa$ were applied.

C. Test Case Results

The calculations started from a homogeneous solution. As a check to determine whether fully developed flow in time was reached or not, the wall friction was calculated in a region at the back of the bump and averaged in spanwise and streamwise direction. When no long time transients could be seen, the flow was considered stable. Data was then averaged for about 5 FTTs, which in real time is $7.5\ ms$. Tests showed that using the semi-implicit preconditioning required about $40\ \%$ of the computational time compared with using the fully explicit scheme.

Figure (8) shows a Mach number contour plot. Both the boundary layer and the shock are clearly visible. In the measurements, a λ-shock can be seen, but no such phenomena was detectable in the results from the calculation. Measurements also revealed boundary layer separation and a recirculation bubble which our calculation captures although the separation seems to be stronger in the measurements. The main reason for the differences is probably the difference in Reynolds number but some can be addressed to the resolution which is on the low side with $\Delta x^+ \sim 150$, $\Delta y^+ \sim 1.5$ and $\Delta z^+ \sim 40$. Also, the domain is probably a bit narrow for the flow structures. Research on this subject is on-going. Some of the Reynolds stresses are shown in figure (9). Notice that the bump is rescaled in the

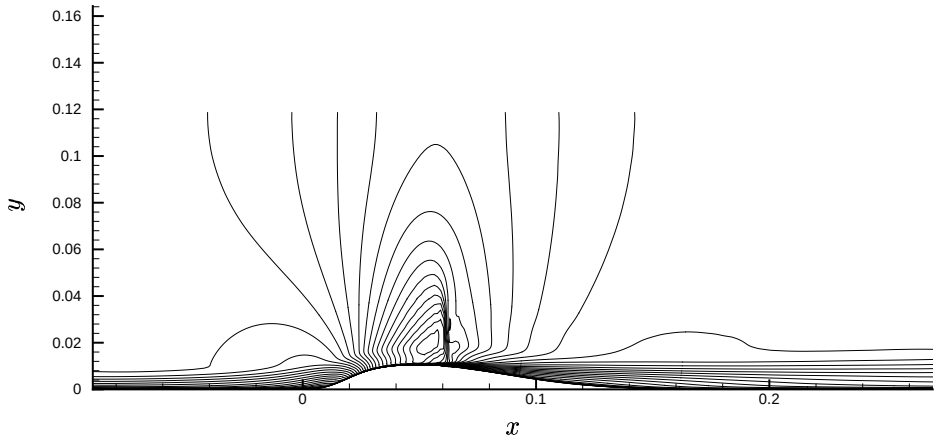

Figure 8. Mach number plot.

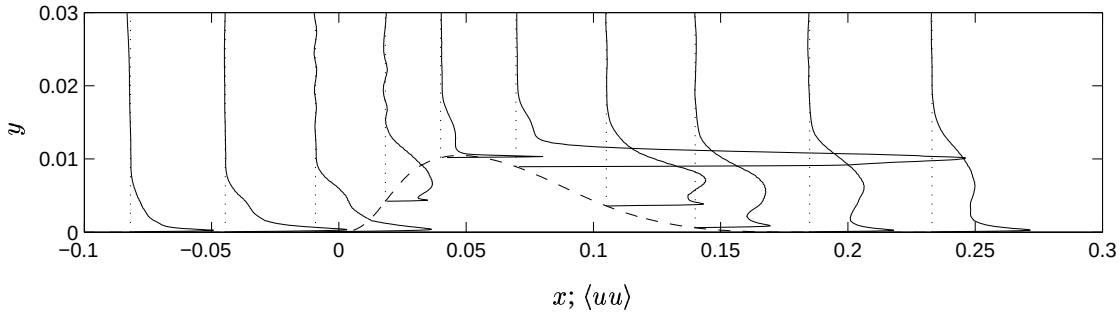

Figure 9. The $\langle uu \rangle$ Reynolds stresses for the test case.

y-direction to fit the scale of the stresses. At the top of the bump, the boundary layer is almost, but not completely, laminarized. Directly after the shock, the Reynolds stresses are very large. One explanation could be that the shock is moving which can be seen in the experimental rig. Animations of the computation show that the shock foot position is not stable, but apart from the fact that detachment occurs, the complexity of the flow pattern hinder conclusions to be drawn without further research. The reattachment at the back of the bump is also visible.

Figure (10) shows a close up of the pressure contours below the shock. As can be seen, no discontinuities or sudden changes can be seen in the region around the interface between the semi-implicit scheme and the fully explicit scheme.

Since no comparison have been made, neither with other calculations nor with experimental data, conclusions about the accuracy of the test case calculation are yet to be made. However, the results so far are sufficient to show that the current semi-implicit method can be applied even to difficult cases like this transonic flow.

VI. Possible Development of the Method

In this work we have chosen a simple implementation, but there are alternatives that will be discussed here.

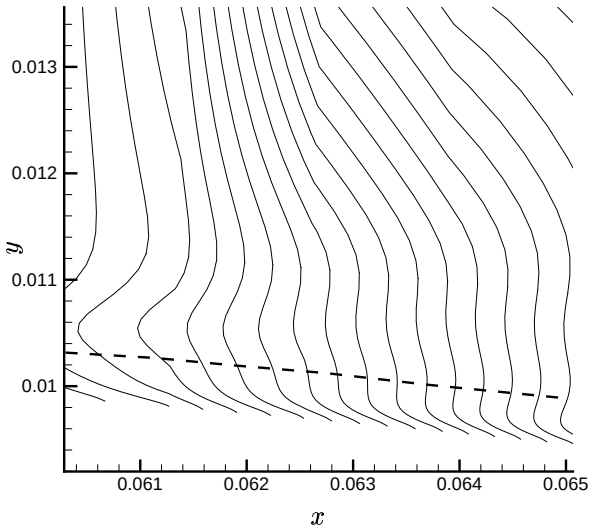

Figure 10. Pressure contours close to the wall beneath the shock. The dashed line indicates the approximate limit for use of the semi-implicit preconditioning. Notice the strong close-up.

First of all, a check of the assumption that the wall normal direction is the by far largest contributor to the CFL-number can be added. Such a check would guaranty that the scheme is only used where the underlying assumptions are valid. The problem is to know what is meant by 'by far largest contributor'. There is probably some practical limit that can be found by testing. We have not tried to find this limit, but know that among the cells for which semi-implicit preconditioning was used, the aspect ratio between the y- and z-direction was about 5 at its smallest value. This can seem low, but these cells were the ones at the outer edge of the columns. Here the influence of the preconditioning is so weak, that a small violation of the assumption introduces no large errors. As a matter of fact the present method is valid for all cells, as long as the CFL-number is less than the limit set by the explicit time stepping method. The only effect will then be a time stepping scheme which is different in one direction compared to the others.

Regarding the performance, tests shows that if the column is 18 cells high, the cells in the column require seven times more computational time than with no preconditioning. Thus, there is much time to save if the preconditioning processing can be made faster. The tests also reveal that calculating the flux Jacobian matrices and solving the resulting equation system require approximately the same time. A high stretching of the cells close to the wall makes the columns shorter and thus less flux Jacobian matrices have to be computed and the resulting equation systems will be smaller and thus faster to solve.

In this work, a direct solver has been used to solve the equation systems for the columns. It utilizes the band structure of the system. Actually the system is penta block diagonal. If a direct solver which utilizes that can be found there would be some gain in performance. Another alternative is to use an iterative solver. The problem is that the system, even though it is block diagonal, is not very sparse. It has a density of about 30 %. Futhermore it possesses non of the desirable properties: It is not symmetric, nor is it positive semi-definite and on top of that, it is often ill-conditioned. The calculations should not stop just because the iterative solver cannot converge. Thus, a direct solver is a more stable choice.

As described in subsection III.D, the flux Jacobian matrices are recalculated for each

stage in the Runge-Kutta method. It has not been tested, but it might be possible to omit this recalculation and instead calculate them only once and reuse that result in all three stages. Another untested possibility is to use a flux scheme of lower order for calculating the flux Jacobian matrices. The risk with such alternations is that they make one Newton-Raphson iteration insufficient and that more iterations must be made. It is not necessary that such an approach will decrease the performance. When we lower the order of the discretization scheme, the band-width of the equation systems will also decrease which makes the systems faster to compute and to solve. So making two iterations with a lower order scheme might be faster and perhaps more accurate than making one iteration with a scheme of higher order.

Last it might be worth pointing out that the present method can be modified to use variable time step. For fully explicit schemes, the maximum time step for all cells are calculated and compared. The smallest of all time steps is then used for all cells. For the present method, when the smallest possible time step is to be found, all cells which can be part of a column should be omitted. The problem is to know which cells that can be part of a column, since that is determined by the limit discussed in the beginning of this section.

VII. Summary

A numerical method based on semi-implicit treatment of the discretized Navier-Stokes equations for compressible flow has been developed. Knowing in advance what cells in the domain that limit the time step, a preconditioning equation for these cells has been derived from the finite volume formulation of the Navier-Stokes equations and applied to LES calculations. The method is, for the cells where it is applied, equivalent to making one iteration with the Newton-Raphson method and also equivalent of making partial factorization, but in one direction only.

The method was validated for developing channel flow where almost perfect agreement between the fully explicit scheme and the semi-implicit preconditioning scheme could be found. In the validation case, the new method saved $40\ \%$ of the computational time compared to the fully explicit scheme.

The new method was also applied to transonic flow over a bump. The results was of physical nature as far as the grid resolution allowed, but the calculation showed anyhow that the new scheme can handle more difficult flow cases. In this case, about $60\ \%$ of the computational time was saved.

The method has potential for further development. It can be made more secure to users mistake and some alterations are possible that might give the method higher performance.

Acknowledgments

This project is sponsored by the Swedish Energy Agency and is a cooperation with the Royal Institute of Technology which has provided us with data for the transonic test case. Thanks to all employees of the Division of Thermo and Fluid Dynamics on Chalmers University of Technology for contributing with valuable ideas and inspiration.

References

[1]**Dolling, D. S., "Fifty Years of Shock-Wave/Boundary-Layer Interaction Research: What Next?" *AIAA Journal*, Vol. 39, No. 8, 2001, pp. 1517 – 1531.**

[2]**Knight, D., Yan, H., Panaras, A. G., and Zheltovodov, A., "Advances in CFD prediction of shock wave turbulent boundary layer interactions," *Progress in Aerospace Science*, Vol. 39, 2003, pp. 122 – 184.**

[3]**Thivet, F., Knight, D., Zheltovodov, A., and Maksimov, A., "Insights in Turbulence Modeling for Crossing-Shock-Wave/Boundary-Layer Interactions," *AIAA Journal*, Vol. 39, 2001, pp. 985 – 994.**

[4]**Davidson, L., "Reynolds stress transport modelling of shock-induced separated flow," *Computer***

& *Fluids*, Vol. 24, 1995, pp. 253 – 268.

[5]**Dong, H. and Zhong, X., "High-Order Semi-Implicit Schemes for Unsteady Compressible Flow Simulations," *AIAA Journal*, Vol. 40, 2002, pp. 869 – 878.**

[6]**Bussing, T. R. and Murman, E. M., "Finite-Volume Method for the Calculation of Compressible Chemically Reacting Flows," *AIAA Journal*, Vol. 26, 1988, pp. 1070 – 1078.**

[7]**Eriksson, L.-E., "Development and validation of highly modular flow solver versions in g2dflow and g3dflow," Internal report 9970–1162, Volvo Aero Corporation, Sweden, 1995.**

[8]**Erlebacher, G., Hussaini, M. Y., Speziale, C. G., and Zang, T. A., "Toward the large-eddy simulation of compressible turbulent flows," *Journal of Fluid Mechanics*, Vol. 238, 1992, pp. 155 – 185.**

[9]**Wollblad, C., "Large eddy simulations of transonic flow with shock wave/turbulent boundary layer interactions," Thesis for licentiate of engineering, in progress, Department of Thermo and Fluid Mechanics, Chalmers, Sweden, 2004.**

[10]**Hoffmann, K. A. and Chiang, S. T., *Computational fluid dynamics for engineers volume II*, Engineering Education System, Wichita, Kansas, USA, 1993.**

[11]**Eriksson, L.-E., "Transfinite Mesh Generation and Computer-Aided Analysis of Mesh Effects," Thesis for the degree of doctor of philosophy, Department of Computer Sciences, Uppsala University, Sweden, 1984.**

[12]**Larsson, J., "Numerical Simulation of Turbulent flows for Turbine Blade Heat Transfer Applications," Thesis for the degree of doctor of philosophy, Department of Thermo and Fluid Dynamics, Chalmers University of Tachnology, Sweden, 1998.**

[13]**Press, W. H., Teukolsky, S. A., Vetterling, W. T., and Flannery, B. P., *Numerical Recipes in Fortran*, Cambridge University Press, 1992.**

[14]**Andersson, N., "A Study of Mach 0.75 Jets and Their Radiated Sound Using Large-Eddy Simulation," Thesis for licentiate of engineering, Department of Thermo and Fluid Mechanics, Chalmers, Sweden, 2003.**

[15]**Sigfrids, T., "Hot wire and PIV studies of transonic turbulent wall-bounded flows," Thesis for licentiate of engineering, Department of Mechanics, Royal Institute of Technology, Sweden, 2003.**

[16]**Bron, O., "Investigation of Air Flow Quality in a VM100 Wind Tunnel, Part1: Relative comparison of the imposed perturbations and the inherent pressure fluctuations." Report, Department of Mechanics, Royal Institute of Technology, Sweden, 2002.**

[17]**Welty, J. R., Wicks, C. E., and Wilson, R. E., *Fundamentals of Momentum, Heat, and Mass Transfer*, John Wiley & sons, New York, USA, 1984.**

[18]**Johansson, G. and Castillo, L., "LDA measurements in turbulent boundary layers with zero pressure gradient," *Proc. Turbulence and Shear Flow Phenomena, 2^{nd} International Symposium*, Stockholm, 2001, pp. 15 – 20.**

[19]**Schlichting, H., *Boundary-Layer Theory, seventh edition*, McGraw-Hill Book Company, New York, USA, 1979.**